

pubs.acs.org/synthbio Research Article

# Genetically Encoded Detection of Biosynthetic Protease Inhibitors

Levi Kramer, Ankur Sarkar, Tom Foderaro, Andrew L. Markley, Jessica Lee, Hannah Edstrom, Shajesh Sharma, Eden Gill, Matthew J. Traylor, and Jerome M. Fox\*



Cite This: ACS Synth. Biol. 2023, 12, 83-94



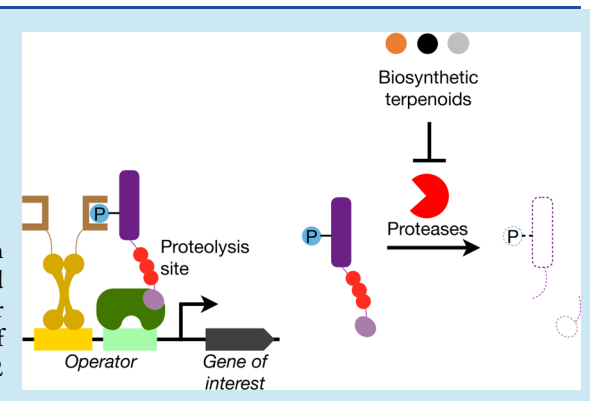
**ACCESS** I

III Metrics & More

Article Recommendations

Supporting Information

ABSTRACT: Proteases are an important class of drug targets that continue to drive inhibitor discovery. These enzymes are prone to resistance mutations, yet their promise for treating viral diseases and other disorders continues to grow. This study develops a general approach for detecting microbially synthesized protease inhibitors and uses it to screen terpenoid pathways for inhibitory compounds. The detection scheme relies on a bacterial two-hybrid (B2H) system that links protease inactivation to the transcription of a swappable reporter gene. This system, which can accommodate multiple biochemical outputs (i.e., luminescence and anti-biotic resistance), permitted the facile incorporation of four disease-relevant proteases. A B2H designed to detect the inactivation of the main protease of severe acute respiratory syndrome coronavirus 2 enabled the identification of a terpenoid inhibitor of modest potency.



An analysis ofmultiple pathways that make this terpenoid, however, suggested that its production was necessary but not sufficient to confer a survival advantage in growth-coupled assays. This finding highlights an important challenge associated with the use of genetic selection to search for inhibitors—notably, the influence of pathway toxicity—and underlines the value of including multiple pathways with overlapping product profiles in pathway screens. This study provides a detailed experimental framework for using microbes to screen libraries of biosynthetic pathways for targeted protease inhibitors.

KEYWORDS: natural products, non-ribosomal peptide synthetases, biological selection, viral proteases, SARS-CoV-2

## **■ INTRODUCTION**

Proteases are centrally important to many biochemical processes and have provided a rich set of targets for treating human These enzymes, which catalyze the hydrolysis of peptide bonds, coordinate the dynamic remodeling-and functional rewiring—of the complex protein systems that underlie blood clotting,<sup>2</sup> tissue repair,<sup>3</sup> and viral assembly,<sup>4</sup> among other biochemical feats.<sup>5–10</sup> The first clinically approved protease inhibitor targeted HIV-1 protease (HIVpro), which cleaves polyproteins into functional subunits of the HIV virion; today, this enzyme is the target of 10 approved drugs. 11 Over the years, proteases have emerged as important targets for other viral diseases—notably, hepatitis C12 and coronavirus infectious disease-19 (COVID-19)13—as well as cardiovascular disorders<sup>14</sup> and cancer.<sup>15</sup> Despite their therapeutic promise, proteases often evolve resistance mutations, which can emerge early in clinical trials, 16 and remain subject to the same slow development timelines that plague other drugs.<sup>17</sup> New approaches for discovering protease inhibitors could help address these challenges.

Natural products are a longstanding source of pharmaceuticals and bioactive compounds, including protease inhibitors, <sup>18,19</sup> but have proven challenging to screen in high-throughput assays. <sup>20</sup> Their low natural abundance and complex biological matrices (i.e., multi-component extracts) often

complicate compound detection and dereplication, <sup>21</sup> while their chemical structures, which often include multiple stereocenters, tend to slow scale-up and hit optimization. <sup>22</sup> Advances in microbial genetics and bioinformatics have led to an explosion of new biosynthetic gene clusters <sup>23–25</sup> and uncovered enzymes capable of adding biochemically nonstandard functionalities (e.g., terminal alkynes, halogens, and hydrazines). <sup>26–28</sup> Unfortunately, the structures and biological activities of biosynthetic compounds remain challenging to predict from sequence data alone, and functional characterization typically requires laborious extraction and purification steps. <sup>29</sup>

Microbial hosts equipped with genetically encoded detection systems offer a promising means of accelerating the discovery of pharmaceutically relevant natural products. These in vivo systems link the inhibition of a heterologously expressed target enzyme to a biochemical output (e.g., growth, color formation, or fluorescence).<sup>30,31</sup> They have several important advantages

Received: July 19, 2022 Published: December 27, 2022





over in vitro assays:<sup>32–35</sup> (i) they can screen DNA-encoded pathways, where library size is limited by transformation efficiency.<sup>36</sup> (ii) They require only a small amount of target protein, which is maintained by a living cell, and can avoid the laborious protein purification and stabilization steps required for in vitro assays.<sup>37</sup> (iii) They are designed to detect inhibitors within the cellular milieu and can thus provide an initial—if, largely, general—screen for inhibitor stability and toxicity.<sup>38</sup> (iv) They can accelerate scale-up of molecular synthesis via microbial fermentation.<sup>39</sup>

Genetically encoded biosensors for enzyme inhibitors are sparse; to date, most have focused on controlling cell viability. Illustrative strategies for protease inhibitors include (i) the addition of protease recognition (PR) sites to antibiotic resistance proteins (e.g., the metal-tetracycline/H+ antiporter) $^{40}$  or essential regulatory enzymes (e.g., adenylate cyclase, which synthesizes cyclic AMP) $^{41}$  or (ii) the use of proteolyzable "pro" domains to cage toxic proteins (e.g., ribosomal protein S12, which restores the streptomycin sensitivity of streptomycin-resistant *E. coli*). Several of these systems have been used to detect peptide inhibitors synthesized in microbial hosts; their direct modification of phenotype-specific proteins (e.g., the adenylate cyclase), however, tends to limit their rapid extension to other proteases and biochemical outputs.

This study develops a general approach for detecting protease inhibitors in microbial hosts. It focuses on four proteases: (i) HIVpro, (ii) the main protease (3CLpro) of severe acute respiratory syndrome coronavirus 2 (SARS-CoV-2), (iii) the papain-like protease (PLpro) of SARS-CoV-2, and (iv) ubiquitin-specific-processing protease 7 (USP7). These enzymes, which are important targets for viral diseases (HIVpro, 43 CLpro, 45 and PLpro) 46 and cancer (USP7), 47 exhibit different yields when overexpressed in *E. coli* and have PR motifs that range from 4 to 75 amino acids. 48–51 Our study begins by using these disparate proteases to develop a general framework for biosensor development and concludes with an exemplary application—the detection of an endogenously synthesized inhibitor of 3CLpro. The study provides a new approach for using microbes to find natural products that inhibit proteases.

## RESULTS

#### Selection of an Initial Bacterial Two-Hybrid System. To

begin, we sought a transcriptional system that links protease inactivation to the expression of a gene of interest (GOI) in *E. coli*. Transcription-based detection systems are advantageous because transcription, translation, and biocatalytic production of a signal (if the gene product is an enzyme) are amplification reactions; at each step, a single biomolecule (i.e., one gene, mRNA, or enzyme) can generate many more, allowing a single transcriptional activator to trigger a signaling cascade. In prior work, we developed a bacterial two-hybrid (B2H) system in which a phosphorylation-mediated binding event activates transcription of a GOI (Figure 1A), and we used it to detect phosphatase inhibitors. This system served as a starting point for the present study.

We started our work by selecting a general detection architecture. Two protein fusions form the core of the base B2H: (i) a Src homology 2 (SH2) domain fused to the cI repressor and (ii) a kinase substrate domain (MidT) fused to the omega subunit of RNA polymerase (RpoZ). Src-mediated phosphorylation of the substrate domain allows it to bind to the SH2 domain, and the resulting substrate—SH2 complex activates transcription of the GOI by localizing RNA polymerase

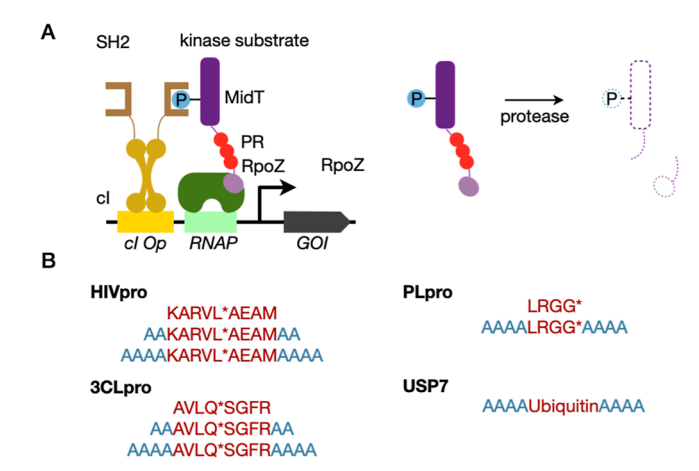


Figure 1. Design of a B2H system that detects protease inhibition. (A) B2H system that links protease inhibition to the expression of a GOI. Major components include (i) a kinase substrate (dark purple) fused to the omega subunit of RNA polymerase (light purple), (ii) a PR site (red), (iii) a Src homology 2 (SH2) domain (dark brown) fused to the 434 phage cI repressor (light brown), (iv) an operator for 434cI (yellow), (v) a binding site for RNA polymerase (light green), (vi) the other subunits of RNA polymerase (dark green), and (vii) the GOI. Src kinase and protein tyrosine phosphatase 1B (PTP1B), which can be encoded by the same plasmid, activate or inhibit the SH2—substrate interaction through phosphorylation and dephosphorylation, respectively. Proteolysis of the PR site disrupts activation. (B) PR sites examined in this study.

to its promoter; PTP1B-mediated dephosphorylation of the substrate prevents this activation. We speculated that this delicate system might respond to protease overexpression, even in the absence of recognition sites; indeed, 3CLpro overexpression reduced GOI transcription (Figure S1). Next, we used 3CLpro to evaluate two different binding pairs: a phosphorylation-dependent pair (SH2/MidT: Figure S1A) and a phosphorylation-independent pair (SH2<sub>ABI</sub>/HA4; Figure S1B).<sup>54</sup> Briefly, we placed 3CLpro on an arabinose-inducible plasmid and tested each pair-specific B2H system with a luminescent reporter (GOI = LuxAB). For both systems, overexpression of an active protease—but not an inactive protease—reduced luminescence. The phosphorylation-independent pair yielded a larger dynamic range (i.e., DR, the change in luminescence caused by protease expression;  $10.7 \pm 1.2$  vs 6.3± 0.9; Figure S1C) but exhibited a higher background signal; when we swapped the GOI with a resistance gene (SpecR), this background allowed the inactive B2H to confer substantial antibiotic resistance—an undesirable result (Figure S1D). We continued sensor development with the phosphorylationdependent binding pair.

Development of B2H Systems that Detect Protease Inhibition. We speculated that the addition of a PR site to the substrate-RpoZ fusion might render it susceptible to proteolysis and enhance the DR associated with protease inactivation. Starting with our base B2H, we explored this idea by adding PR sites for HIVpro and 3CLpro, each flanked by 0–4 alanine residues (Figure 1). These sites reduced the DR associated with PTP1B inactivation by up to two-fold, relative to PR-free systems, but retained the original B2H activity (i.e., PTP1B inactivation increased luminescence; Figure 2A). Next, we supplemented 0- and 4-alanine versions of the modified B2Hs with active proteases, which we overexpressed from a second plasmid.

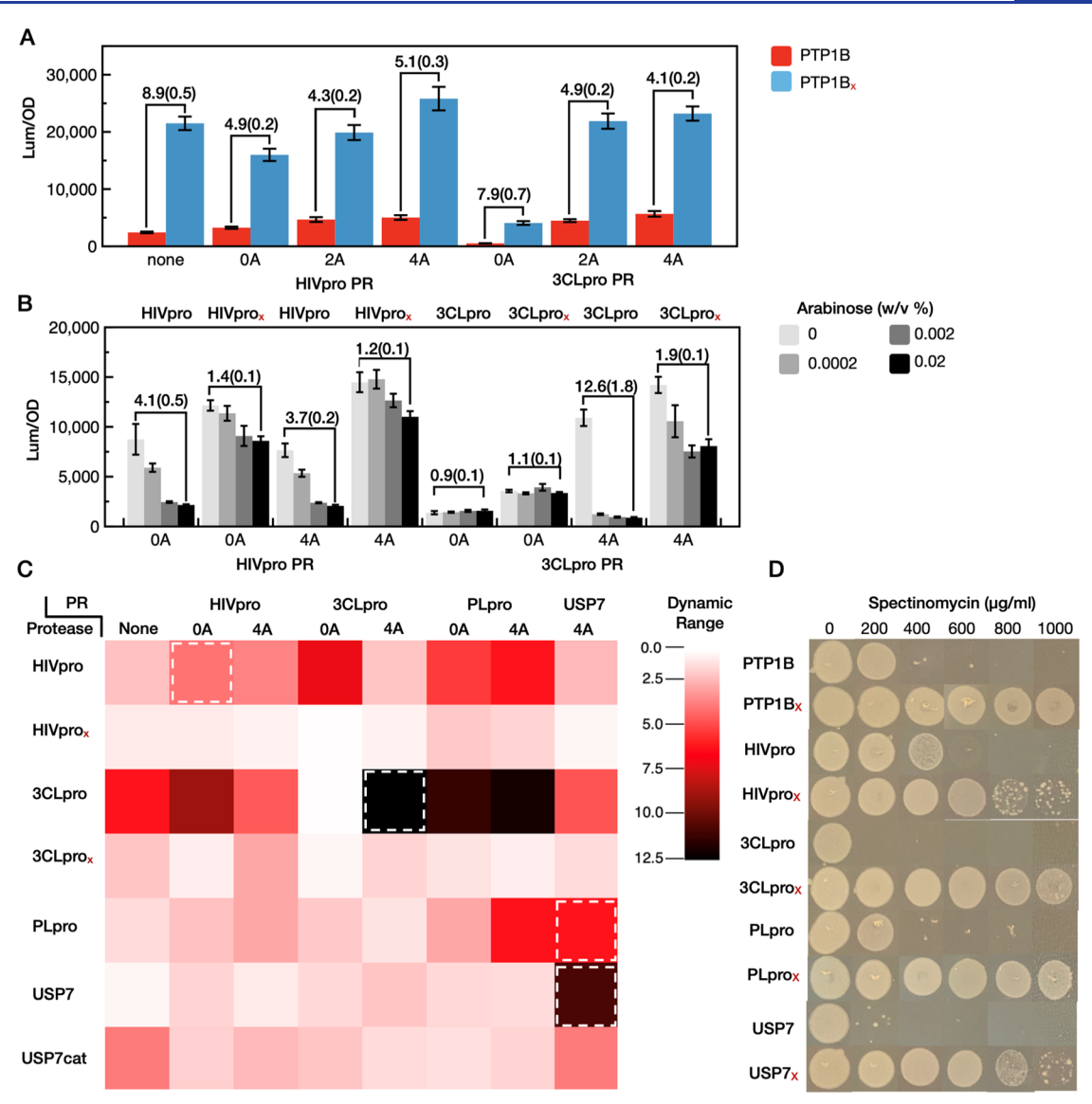


Figure 2. Development of protease-specific B2H systems. (A) B2H systems that link PTP1B inactivation (C215S) to a luminescent output (LuxAB expression). We added PR sites flanked by alanine (A) residues to the linker that connects MidT to the omega subunit of RNA polymerase (Figure 1). Their addition reduces the dynamic range (DR, the difference in fluorescence between active and inactive variants of PTP1B). (B) We used a pBAD plasmid to titrate active and inactive proteases alongside the constitutively active B2H systems from A (i.e., the PTP1B C215S systems). For 3CLpro, the four-alanine linker exhibited the highest DR; for HIVpro, the DRs afforded by zero- and four-alanine linkers were not statistically significant (p < 0.05). (C) We used the two-plasmid system from B to screen proteases against different PR sites. The dynamic range corresponds to the difference in luminescence between 0 and 0.02 w/v % arabinose. "None" denotes systems that lack a PR site, a baseline for comparing the improved DR afforded by these sites. The white squares show the PR sites of the final B2H systems. (D) We modified the PTP1B-based B2H system from A by (i) swapping in proteases for PTP1B, (ii) adding the highlighted PR sites from C, and, where necessary, (iii) adjusting the RBSs for protease genes. Images show the growth of *E. coli* harboring protease-specific B2H systems on agar plates seeded from drops of liquid culture (*E. coli* S1030 + pB2H; LB agar, pH 7.5). In all panels, X denotes inactive variants of each protease: PTP1B (C215S), 3CLpro (H41A), HIVpro (D25N), USP7 (C223S), and PLpro (C111S). Figure S2 provides detailed schematics for the B2H systems used in the experiments described by each panel of this figure. Data points denote the mean and standard error of  $n \ge 6$  technical replicates.

Enzyme overexpression reduced luminescence for both HIVpro systems but only one 3CLpro system (the 4-alanine version; Figure 2B); as expected, the inclusion of PR sites improved the DR associated with protease inactivation, relative to the PR-free systems (Figure 2C). Intriguingly, inactive proteases also caused a slight reduction in luminescence (Figure 2B,C), an effect that might reflect proteases binding to PR sites (and subsequent disruption of B2H function) or a general cellular response to protein overexpression. Nonetheless, our results indicate that PR sites can enhance the sensitivity of B2H systems to protease activity.

Our work with HIVpro and 3CLpro illustrates how two genetic modules—a luminescent B2H and an arabinose-inducible protease—enable titration experiments that facilitate the rapid evaluation of different protease—PR combinations. We used this two-module luminescent system to expand our screen of PR sites to different proteases (Figure 2C). In short, we added PR sites for HIVpro, 3CLpro, PLpro, and USP7 to the substrate—RpoZ fusion and evaluated the response of each system to protease overexpression. We note that both PLpro and USP7 remove ubiquitin, <sup>55</sup>,56 but PLpro recognizes its terminal LRGG sequence, <sup>57</sup> so we included this sequence as a separate

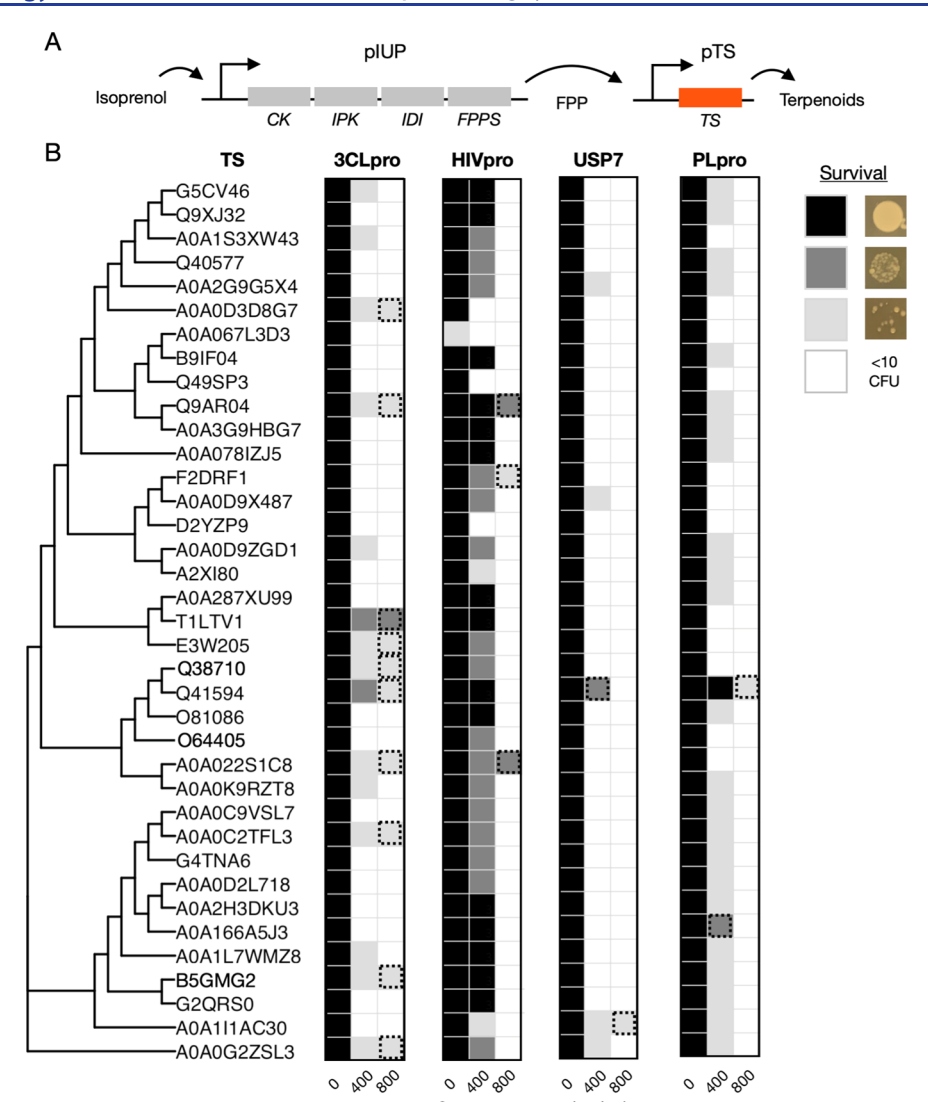


Figure 3. Screen of terpenoid pathways. (A) Plasmid-borne pathway for terpenoid biosynthesis: (i) pIUP, which converts isoprenol to farnesyl diphosphate (FPP), and (ii) pTS, which encodes a TS. Genes: choline kinase and isopentenyl diphosphate isomerase (IDI) from *S. cerevisiae*, FPP synthase (FPPS) from *E. coli*, and isopentenyl phosphate kinase from *A. thaliana*. (B) We transformed *E. coli* with three plasmids—a protease-specific B2H system (pB2H), pIUP, and pTS—and used the transformed strains to screen 37 phylogenetically distinct TSs for their ability to enhance spectinomycin resistance. The TSs are grouped by lines of inferred evolutionary decent (a phylogenetic tree). Dashed boxes: terpenoid pathways that conferred the greatest resistance for each B2H. Figure S8 shows original data. In the rescreen, Q41594 (orange box) conferred the most consistent survival advantage for the 3CLpro system. (*E. coli* S1030 + pB2H + pIUP\_FPPS + pTS; LB agar with 2% glycerol, 10 mM isoprenol, and 50 μM IPTG, pH 7.0).<sup>76</sup>

site. For USP7, we included the catalytic domain with and without a C-terminal extension that stabilizes its catalytically competent conformation. Consistent with their reported substrate specificities, 3CLpro, PLpro, and USP7 reduced luminescence most significantly when paired with cognate PR sites, while HIVpro appeared functional with all sites—a behavior that matches its reported promiscuity. The extended version of USP7 yielded the highest DR (>10-fold) on ubiquitin. Considering this impressive DR, which was produced by a 4-alanine linker, and the size of ubiquitin, which is large relative to the other PR sites (i.e., 75 vs 4–9 amino acids), we chose not to test a zero-alanine linker with this protein. We selected the native PR sites (with 0- or 4-alanine flanking regions) to complete B2H development.

We constructed single-plasmid B2H systems by making three modifications to our base system: we (i) exchanged the gene for PTP1B with protease genes, (ii) added the PR sites selected in

our luminescent screen, and (iii) exchanged the luciferase gene (LuxAB) for a spectinomycin resistance gene (SpecR). The B2H for USP7 worked immediately (Figure S3); active USP7 conferred sensitivity to spectinomycin (i.e., death at 200  $\mu$ g/mL spectinomycin), and inactive USP7 yielded resistance (i.e., growth at 800  $\mu$ g/mL spectinomycin). B2Hs for the remaining proteases, by contrast, conferred only mild sensitivity to spectinomycin. We speculated that this insensitivity might result from poor protease expression and thus modified the ribosome binding sites (RBSs) for each protease gene. Indeed, for HIVpro and 3CLpro, a screen of several RBSs with different translation initiation rates yielded variants that enhanced sensitivity to spectinomycin (Figures S4 and S5). For PLpro, we streamlined our RBS screen by using degenerate primers to build a library of 32 variants in a single amplification reaction (Figure S6). With optimized RBSs, the final B2H systems linked

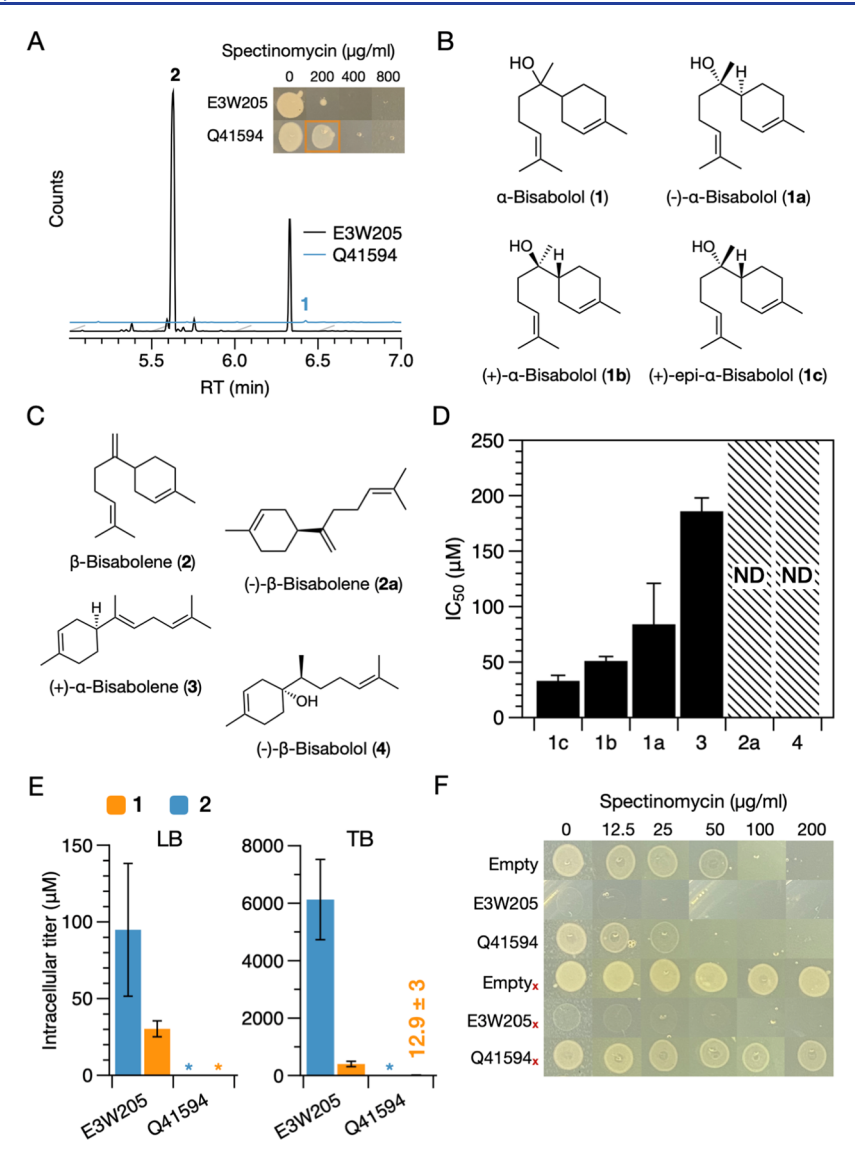


Figure 4. Analysis of terpenoid inhibitors. (A) Sesquiterpene production by E3W205 and Q41594 in liquid culture. Chromatograms show total ion counts for full scans (m/z = 50-350). (*E. coli* DH5α + pAM45 + pTS; TB liquid with 500 μM IPTG). Chromatograms showing terpene production by additional hits from Figure 3, along with several additional TSs included in our screen, appear in Figure S10. Inset: spectinomycin resistance conferred by E3W205 and Q41594 on agar plates in a drop-based assay carried out to follow up on the results of our initial screen (Figure S9 shows the full results of the re-screen). Q41594 yields a prominent survival advantage, relative to E3W205. (B,C) Q41594 generates a small amount of α-bisabolol, which has several commercially available stereoisomers. (C) Bisabolenes produced by various TSs examined in this study. (D) IC<sub>50</sub>s show the inhibition of 3CLpro by various bisabolenes (fluorogenic substrate = TSAVLQ\_AFC). Data show the mean and standard error for  $n \ge 3$  independent estimates (N.D., not determinable). (E) Sensitivity of terpenoid titers to media composition. Intracellular titers of major products of E3W205 and Q41594 in LB or TB liquid media: α-bisabolol (1) and β-bisabolene (2). The orange text denotes the titer of α-bisabolol produced by Q41594 in TB media; \*, no detectable product. Data show the mean and standard deviation for  $n \ge 3$  biological replicates. (*E. coli* S1030 + pB2H\_3CL + pIUP\_FPPS + pTS; LB liquid with 50 μM IPTG and 10 mM isoprenol; TB liquid with 500 μM IPTG and 50 mM isoprenol). (F) This image shows the spectinomycin resistance of B2H-encoded *E. coli* cells harboring different TS genes. We seeded cells by dropping TB liquid culture onto LB agar plates (i.e., LB agar with 2% v/v glycerol, 1000 μM IPTG, and pH 7.0 supplemented with antibiotics); X denotes inactive 3CLpro (H41A). Note: these strains contain no FPP pathway. The resistance conferred by E3W205 and Q41594 decreased, relative to Figure 1A. E3W205 reduced cell survival, even in the presence o

protease inactivation to a major improvement in spectinomycin resistance (Figures 2D and S7).

Biosynthesis of Terpenoid Inhibitors. We evaluated the potential for our B2H systems to find unexpected inhibitors by using them to screen terpenoid pathways. These pathways generate mixtures of products that are challenging to purify. As nonpolar molecules, terpenoids are also novel—if not necessarily intuitive—scaffolds for building protease inhibitors, which are typically peptide mimics. <sup>59</sup> To simplify our screen, we

assembled each terpenoid pathway with two plasmid-borne modules: pIUP, which converts isoprenol to farnesyl pyrophosphate (FPP), and pTS, which encodes a terpene synthase (TS; Figure 3A). By swapping out the second module, we examined 37 phylogenetically diverse TSs selected in a prior analysis of 8 clades of the largest TS gene family (PF03936; Figure 3B);  $^{53}$  this set includes TSs that act on  $C_{10}$ ,  $C_{15}$ , and  $C_{20}$  linear isoprenoids (geranyl pyrophosphate, or GPP; FPP; and geranylgeranyl pyrophosphate, or GGPP, respectively) as well as uncharac-

terized TSs. TSs are notoriously promiscuous, <sup>60,61</sup> so we speculated that some of these enzymes might generate products from non-native substrates (i.e., FPP). To carry out our screen, we searched for pathways that improved the antibiotic resistance of B2H-encoded *E. coli*. In the first screen, the 3CLpro-specific B2H yielded the most hits (Figures 3 and S8). 3CLpro is an important target for treating COVID-19 and other coronavirus diseases, <sup>62,63</sup> so we focused on this enzyme for the remainder of our analysis.

We whittled down our initial hits in two steps. First, we examined their product profiles in liquid culture by pairing each TS with a plasmid harboring the mevalonate-dependent isoprenoid pathway from Saccharomyces cerevisiae (pAM45); this pathway affords high titers of sesquiterpenes in E. coli and, thus, facilitates TS characterization. Of nine initial hits, five generated products detectable with gas chromatography-mass spectrometry (GC-MS) (Figure S10). We speculate that the unproductive TSs-which include T1LTV1, a TS that conferred a prominent survival advantage in our initial assay are false positives or have productivities that are highly sensitive to culture conditions. Next, we re-screened all hits in biological triplicate (Figure S9). One yielded a consistent survival advantage (i.e., reproducible growth at higher antibiotic concentrations than other TSs): Q41594, a taxadiene synthase from Taxus brevifolia. This enzyme natively converts GGPP to taxadiene, but it can generate bisabolenes from FPP. 64 In our hands, it produced a small amount of  $\alpha$ -bisabolol (Figure 4A). We focused further characterization on this compound.

In vitro kinetic assays allowed us to examine the inhibitory effect of  $\alpha$ -bisabolol. The small amount of this compound produced by Q41594 in liquid culture was difficult to purify, so we tested three commercially available diastereomers:  $(-)-\alpha$ bisabolol, (+)- $\alpha$ -bisabolol, and (+)-epi- $\alpha$ -bisabolol. These compounds had similar IC<sub>50</sub>s, which ranged from 30  $\pm$  5 to  $80 \pm 36 \mu M$ , a range consistent with the  $K_i$ s of inhibitors identified with previous genetic screens (Figures 4D and S11). S3,65,66 These IC $_{50}$ s confirm that Q41594 can generate inhibitors of 3CLpro; nonetheless, they are surprising for two reasons: (i) they are higher than the intracellular titer of  $\alpha$ bisabolol produced by Q41594 in liquid culture, and (ii) they are similar to—or lower than—the intracellular titer afforded by E3W205, a  $\beta$ -bisabolene synthase that confers less antibiotic resistance than Q41594 (Figure 4E). Of course, intracellular titers can vary with media conditions (as observed between LB and TB in Figure 4E) and may differ on agar plates. Nonetheless, the lack of a simple correlation between  $\alpha$ -bisabolol production and antibiotic resistance indicates that  $\alpha$ -bisabolol, alone, is insufficient to explain the survival advantage afforded by Q41594.

Prior work on TSs suggests that they can exhibit different toxicities in *E. coli*, even in the absence of isoprenoid pathways and/or active B2H systems <sup>67,68</sup>—perhaps, a result of differences in protein expression or solubility. To evaluate the contribution of TS toxicity to the fitness advantage conferred by Q41594, we carried out two experiments. In the first, we transformed *E. coli* with plasmids harboring Q41594, E3W205, and "no gene" (i.e., an empty TS vector) and grew the transformed strains in liquid culture (Figure S12A). These cells contained neither the FPP pathway nor the B2H system, so differences in terpenoid production and 3CLpro inhibition between strains should be negligible. To our surprise, the Q41594 strain exhibited the lowest specific growth rate, which suggests that this TS does not improve antibiotic resistance

solely by reducing protein toxicity. Growth in liquid culture, however, causes different cellular stresses than growth on solid media, which we used to screen terpenoid pathways. To examine the toxicity of TSs under conditions that more closely approximate those of our screen, we used drop-based plating (Figure 4F). As before, we left out the FPP pathway to remove the influence of terpenoid biosynthesis, but we retained the B2H system—a potential source of additional stress (e.g., expression of B2H components and the influence of antibiotics for plasmid maintenance). Without an FPP pathway, the resistance conferred by E3W205 and Q41594 decreased dramatically, relative to our initial screen—an indication that B2H activation requires terpenoid production. Strikingly, E3W205 reduced cell survival, even in the presence of an inactive 3CLpro (i.e., a constitutively active B2H that should yield maximal resistance). This finding suggests that E3W205 exhibits a toxicity that is both (i) independent of terpenoid production and (ii) amplified in the presence of the B2H system on solid media. This toxicity may explain the failure of E3W205 to emerge as a hit in our screen of terpenoid pathways.

The influence of enzyme toxicity on cell growth motivates a logical question: would a luminescent screen, where signal is normalized by cell density, supply a better means of screening terpenoid pathways? To assess whether luminescent screens are, indeed, less sensitive to differences in cell growth, we carried out two experiments: first, we examined the DR afforded by our 3CLpro-specific B2H system after different growth times (i.e., growth after subculture inoculation; Figure S13A). Unfortunately, luminescence, even when normalized by OD<sub>600</sub>, was sensitive to culture time; the DR ranged from ~5 to 20. This sensitivity complicates comparisons of strains with different growth rates. Next, we examined the luminescence afforded by inactive 3CLpro, which should yield maximal signal, in the presence of three TSs: Q41594, E3W205, and O64405—a hit and two non-hits (Figure S13B). All three TSs reduced luminescence. This effect may result from the dependence of luminescence on decanal, <sup>71</sup> a metabolic derivative that relies on fatty acid synthesis, which is sensitive to cellular stress.<sup>72</sup> Regardless of its mechanistic basis, this sensitivity precludes the facile extension of luminescent B2H systems to screens of terpenoid pathways.

A handful of well-characterized TSs produce  $\alpha$ -bisabolenes. We used them to expand our analysis of the link between  $\alpha$ -bisabolol production and antibiotic resistance. In a screen of seven additional TSs, two  $\alpha$ -bisabolol producers emerged as hits: (i) A0A1L7NYG3, a (+)- $\alpha$ -bisabolol synthase from Artemisia kurramensis, and (ii) J7LH11, a (+)-epi- $\alpha$ -bisabolol synthase from Phyla dulcis (Figure S14). Interestingly, two other  $\alpha$ -bisabolol producers failed to improve resistance: A0A118JXI9, a (-)- $\alpha$ -bisabolol synthase from Cynara cardunculus, generated more  $\alpha$ -bisabolol than the survival-enhancing J7LH11, and (ii) G8H5N1, a sesquiterpene synthase from Solanum habrochaites, produced less (in liquid culture; Figure S15A). As in the first screen, the product profile was an imperfect predictor of survival advantage.

We completed our analysis of bisabolene producers by examining the inhibitory effects of three other compounds produced by TSs included in our screen (Figure 4C):  $\alpha$ -bisabolene,  $\beta$ -bisabolene, and  $\beta$ -bisabolol. For this test, we selected stereoisomers that we could purchase or easily purify from liquid culture. Intriguingly,  $\alpha$ -bisabolene was less inhibitory than  $\alpha$ -bisabolol (IC<sub>50</sub> = 186  $\pm$  12  $\mu$ M), and the inhibitory effects of  $\beta$ -bisabolene and  $\beta$ -bisabolol were too weak

to yield accurate IC $_{50}$  estimates ( $\leq$ 50% inhibition at 1000  $\mu$ M in our initial screen; Figure S11B). These results are consistent with the ability of  $\alpha$ -bisabolol to improve the antibiotic resistance of B2H-encoded cells by inhibiting 3CLpro more effectively than other bisabolene analogues.

The discrepancy in resistance afforded by TSs that produce  $\alpha$ bisabolol has several possible causes. We will list them in an order supported by our data, starting with the most likely: (i) the survival-enhancing TSs that generate  $\alpha$ -bisabolol might be less toxic than other TSs that make the same product. This effect is consistent with the poor growth conferred by E3W205, relative to Q41594, on solid media in the absence of an FPP pathway. (ii) The TS hits might make enough  $\alpha$ -bisabolol to inhibit 3CLpro but not so much that it inhibits other enzymes in the cell and disrupts growth. This "Goldilocks" theory is consistent with the failure of E3W205 and A0A118JXI9, which have high  $\alpha$ bisabolol titers, to emerge as hits in our initial screen and also the emergence of Q41594 as a hit for multiple proteases (Figure 3)—an indication of its potential to generate a general inhibitor; however, it is not supported by the failure of G8H5N1, a TS that generates less  $\alpha$ -bisabolol than the highly productive J7LH11, to confer a survival advantage in our second screen of bisabolene producers. (iii) The TS hits might not make deleterious side products. This theory is consistent with the product profile of E3W205, which generates  $\beta$ -bisabolene as the dominant product, but not with that of A0A118JXI9, a non-hit that makes almost exclusively  $\alpha$ -bisabolol. (iv) The TS hits might produce an undetectable side product that is the true inhibitor of 3CLpro. This mechanism is the most unlikely, given the necessary potency of a minor product (i.e., a low intracellular concentration requires a low IC<sub>50</sub>) and the requirement that it is generated only by TSs that also make  $\alpha$ -bisabolol.

Our findings indicate that  $\alpha$ -bisabolol—the major product of all three hits identified in our screen—can activate the B2H system by inhibiting 3CLpro but suggest that this terpenoid, alone, is insufficient to yield a survival advantage; in particular, the bisabolol-synthesizing TS must be sufficiently non-toxic to avoid inhibiting cellular growth. This finding is consistent with the results of a recent directed evolution experiment in which we used a B2H system to evolve mutants of  $\gamma$ -humulene synthase (O64405) that generate inhibitors of PTP1B; mutants improved resistance both by reducing enzyme toxicity and by enhancing inhibitor production. <sup>73</sup>

## CONCLUSIONS

Proteases are an important class of drug targets that could benefit from new methods for inhibitor discovery. In this study, we developed an approach for using B2H systems to detect protease inhibitors and extended it to four important enzymes. Starting with a phosphorylation-sensitive B2H, which yielded a conveniently low background signal, we added PR sites that caused active proteases to disrupt transcriptional activation. In general, the PR site and protease RBS had the strongest influence on dynamic range; luminescence-based screens facilitated a rapid evaluation of the former; growth-coupled assays, the latter. Methods for screening both components in combination—and, ideally, within the final B2H system intended for use in high-throughput assays—could accelerate the optimization of new protease-specific B2H systems.

Our B2H system has several important advantages over previous biosensors for protease inhibitors: (i) the substrate—RpoZ fusion can accommodate a large range of linker lengths (e.g., the addition of peptide stretches of 4–75 amino acids)

and, thus, facilitates the incorporation of different PR motifs. (ii) It controls the transcription of user-defined GOIs (e.g., genes for luminescence, antibiotic resistance, or, perhaps, fluorescence) and is, thus, compatible with a large variety of high-throughput screens. (iii) It relies on a system of adjustable components—from the PR site and protease RBS, which helped improve the dynamic range in our systems, to the peptide substrate and kinase RBS, which can modulate the extent of protein—protein binding; these components provide multiple routes to B2H optimization. The modularity of our B2H system promises to facilitate its extension to different targets, signals, and assay types.

Our screen of terpenoid pathways highlights important challenges and opportunities for using genetically encoded detection systems. Although we identified a previously unreported terpenoid inhibitor of 3CLpro— $\alpha$ -bisabolol, which has a reasonable IC<sub>50</sub> ( $\sim$ 30-80  $\mu$ M) for a 15-carbon hydrocarbon—the production of this terpenoid alone was insufficient to enhance antibiotic resistance. This finding indicates that simple comparisons of the product profiles of hits and non-hits can miss inhibitory products and, thus, highlights the importance of including multiple pathways that generate the same product in pathway libraries. Curiously, one hit from our screen (Q41594) produced small amounts of  $\alpha$ bisabolol in liquid culture, where intracellular titers were lower than the IC<sub>50</sub>. These titers were sensitive to media composition and thus motivate both (i) the exploration of multiple growth conditions in future screens and (ii) the development of methods for examining terpenoid production under conditions that match those of each screen (e.g., solid media). Intriguingly, Q41594 was a hit for multiple B2H systems, an indication that  $\alpha$ bisabolol may not be selective for 3CLpro. Our B2H systems, after all, require only protease inhibition; nonetheless, our analysis suggests that a side-by-side comparison of multiple, protease-specific B2Hs could facilitate the identification of pathways that generate selective inhibitors (i.e., a pathway that confers a survival advantage for only one system). In the everexpanding search for biologically active natural products, genetically encoded detection systems do not avoid all the challenges of in vitro screens; pathway toxicity can obscure inhibitory metabolites, and dereplication can take time. Variability in the growth or productivity of strains overexpressing terpenoid pathways could also yield false positives or cause some interesting yet media-sensitive pathways to be overlooked. Nonetheless, by whittling down large pathway libraries to a small subset that generate inhibitors, these detection systems can reduce the throughput required for compound isolation and analysis.

## METHODS

Materials. We purchased M9 minimal salts, tris(2-carboxyethyl)phosphine (TCEP), bovine serum albumin, phenylmethylsulfonyl fluoride, 3-methyl-2-buten-1-ol (prenol), dimethyl sulfoxide (DMSO), isopropyl-D-thiogalactopyranoside (IPTG), (-)-α-bisabolol, 3CLpro fluorogenic peptide substrate (TSAVLQ\_AFC), 7-amino-4-trifluoromethylcoumarin (AFC), BugBuster 10X Protein Extraction Reagent, Steriflip filters, and ACS grade hexane from Millipore Sigma; deuterated chloroform from Cambridge Isotope Laboratories (99.8% D); cloning reagents from New England Biolabs; BL21(DE3) pLysS competent cells from Novagen; pGEX-4T-1 GST vector from GenScript; 2.5 L Ultra Yield Flasks from Thomson Instrument Company; antibiotics, media components, pre-made HEPES

buffer (1 M pH 7.3), and human rhinovirus (HRV) 3C protease from Thermo Fisher; lysozyme from Thermo Scientific; imidazole from Teknova; 30 kDa Spin-X UF spin columns from Corning; HisTrap HP and HiTrap Q-HP columns from Cytiva; glycerol, bacterial protein extraction reagent II (B-PERII), and lysozyme from VWR; and (+)- $\alpha$ -bisabolol, (+)-epi- $\alpha$ -bisabolol, (-)- $\beta$ -bisabolol, and (-)- $\beta$ -bisabolene from Toronto Research Chemicals. We prepared a vanillin-sulfuric acid solution by adding 7 g of vanillin and 1.3 mL of concentrated H<sub>2</sub>SO<sub>4</sub> to 200 mL of methanol for TLC visualization.

Cloning and Molecular Biology. We constructed plasmids with Gibson or Golden Gate assembly. Table S1 lists gene sources, Table S2 describes composition of all plasmids, Table S3 lists the DNA sequences of important components, and Table S4 lists primers.

**Bacterial Strains.** This study used several *E. coli* strains. We used chemically competent NEB Turbo cells for molecular cloning, chemically competent or electrocompetent S1030 cells (Addgene no. 105063) for luminescence studies and drop-based plating, DHS $\alpha$  for terpenoid production, and *E. coli* NEB BL21(DE3) for protein overexpression.

We generated chemically competent cells in six steps: (i) we plated cells on LB agar plates with the requisite antibiotics (listed in Table S2). (ii) We used individual colonies to inoculate 5 mL of LB media (25 g/L LB with antibiotics) in glass culture tubes and grew these cultures overnight (37 °C, 225 rpm). (iii) We used 100  $\mu$ L of overnight culture to inoculate 10 mL of LB media (25 g/L LB with antibiotics) in 125 mL shake flasks, which we incubated for several hours (37 °C, 225 rpm). (iv) When the OD<sub>600</sub> reached 0.5–0.8, we centrifuged the cells (4000g, 3 min, room temperature), removed the supernatant, and placed the pellets on ice. (v) We resuspended the pellets in 1 mL of ice-cold solution of 100 mM CaCl<sub>2</sub> and 7% DMSO (sterile-filtered). (vi) We split cells into 100  $\mu$ L aliquots and froze them at -80 °C for further use.

We generated electrocompetent cells by following an approach similar to the one above. In step iv, we resuspended the cells in 1 mL of ice-cold Milli-Q water, then recentrifuged, and resuspended in sterile ice-cold 20% glycerol twice. We froze the pellets as before.

Luminescence Assays. We carried out luminescence assays in seven steps: (i) we transformed S1030 cells with protease-free B2H systems with and without pBAD plasmids listed in Table S2. (ii) For each experiment, we used six colonies to inoculate six 1 mL cultures (terrific broth, or TB, at 2%, or 12 g/L tryptone, 24 g/L yeast extract, 12 mL/L 100% glycerol, 2.28 g/L KH<sub>2</sub>PO<sub>4</sub>,  $12.53 \text{ g/L K}_2\text{HPO}_4$ , pH = 7.3, and antibiotics described in Table S2) in 96-well deep-well blocks and grew the cultures overnight (37 °C, 225 rpm). (iii) We diluted each overnight culture 1:100 in fresh TB (as in ii) with the following arabinose concentrations (% w/v): 0, 0.0002, 0.002, and 0.02. (iv) We incubated each culture for 5.5 h (37 °C, 225 rpm). (v) We added 100  $\mu$ L of each culture to a clear flat-bottom 96-well plate and measured both OD<sub>600</sub> (absorbance at 600 nm) and luminescence (578 nm wavelength, 1000 ms integration, 1.0 mm read height) with a SpectraMax iD3 multi-mode plate reader (Molecular Devices).

Analysis of Antibiotic Resistance. We examined the spectinomycin resistance of B2H-containing strains in six steps: (i) we transformed S1030 cells with pIUP\_FPPS and variants of pTS and pB2H (Table S2), plated the transformed cells on LB agar supplemented with antibiotics for plasmid maintenance (50  $\mu$ g/mL kanamycin, 100  $\mu$ g/mL carbenicillin, 10  $\mu$ g/mL

tetracycline, and 34  $\mu$ g/mL chloramphenicol), and grew them overnight (37 °C). (ii) We used single colonies to inoculate 1 mL of TB (pH = 7.0 supplemented with plasmid antibiotics) and grew the cells overnight (37 °C and 225 rpm). (iii) We diluted an aliquot of each culture 1:100 in TB (as above), and we plated 3  $\mu$ L of the dilution on LB agar plates (pH = 7.0) supplemented with 10 mM isoprenol, 50  $\mu$ M IPTG, 20 mL/L glycerol, antibiotics for plasmid maintenance (as above), and varying concentrations of spectinomycin, unless otherwise specified in our figures. (v) We grew the cells at 22 °C for at least 48–72 h before photographing them.

**Biosynthesis of Terpenoids.** We carried out small-scale terpenoid production in TB (pH = 7.0) supplemented with antibiotics (Table S2). Briefly, we transformed S1030 cells harboring pIUP\_FPPS and pTS, plated the cells on LB agar, and grew them overnight (37 °C). We used colonies to inoculate 2 mL of TB, which we grew overnight (37 °C, 225 rpm); on the next morning, we diluted the culture with TB at a ratio of 1:75 in 10 mL of TB and grew it to an OD<sub>600</sub> of 0.3–0.6 (37 °C, 225 rpm). We induced the culture by adding 10 or 50 mM isoprenol and 500  $\mu$ M IPTG and grew it at 22 °C for 72 h. Table S5 describes exact growth times for the cultures used to estimate intracellular titers (Figure 4A,E).

GC-MS Analysis of Terpenoids. We measured terpenoids generated in liquid culture with GC-MS (a Trace 1310 GC fitted with a TG5-SilMS column, 15 m  $\times$  0.25 mm, film thickness  $0.25 \mu m$ , and an ISQ 7000 MS; Thermo Fisher Scientific). We prepared all samples in hexane and diluted highly concentrated samples 10-20 times prior to bringing concentrations within the MS detection limit. For full scans, we used the following GC method: hold at 40 °C (1 min), increase to 250 °C (30 °C/min), hold at 250 °C (10 min). For the select-ion scans (SIM; Figure S15), we used a 30 m column and modified the GC method: hold at 80 °C (3 min), increase to 250 °C (15 °C/min), hold at  $250 \,^{\circ}\text{C}$  (4 min), increase to  $300 \,^{\circ}\text{C}$  (60  $^{\circ}\text{C/min}$ ), hold at  $300 \,^{\circ}\text{C}$ (1 min). We scanned m/z ratios from 50 to 350 and identified molecules by using the NIST MS library; when necessary, we confirmed this identification with analytical standards or mass spectra reported in the literature. When quantifying terpenoids, we scanned m/z = 204, a mass/charge ratio with a high signal for sesquiterpenes.

To quantify  $\alpha$ -bisabolol and  $\beta$ -bisabolene, we built GC/MS standard curves of structurally similar molecules (Figure S17). We used store-bought (-)- $\alpha$ -bisabolol, and, in the absence of a highly pure analytical standard of  $\beta$ -bisabolene, we used  $\alpha$ -bisabolene isolated from bacterial cultures. We created a series of stocks of both standards in hexane and analyzed them with GC/MS as outlined above.

**Isolation of α-Bisabolene.** We produced α-bisabolene by carrying out the following steps: (i) we transformed *E. coli* DH5α with pAM45 and pTS containing α-bisabolene synthase (Uniprot ID: O81086) and used individual colonies to inoculate six 20 mL starter cultures (TB, pH = 7.0 supplemented with plasmid antibiotics). (ii) We used each starter culture to inoculate a 50 mL culture (i.e., a 1:50 dilution in TB, pH = 7.0), which we grew to an OD of 0.3–0.6 (37 °C, 225 rpm), induced with 500 μM IPTG, and then grew for 144 h (22 °C, 225 rpm). (iii) We combined the six 50 mL cultures with 90 mL hexanes and agitated it at room temperature for 30 min (vortexer). (iv) We used a separatory funnel to remove the hexanes and added them to a 500 mL centrifuge tube, which we spun at 4000 rpm for 20 min. (v) We moved the supernatant to a round-bottom flask and evaporated the hexanes under vacuum to produce

crude oil. (vi) We loaded 71.4 mg of crude oil onto a 5 g silica column (Sigma) and removed the non- $\alpha$ -bisabolene components with vacuum liquid chromatography (VLC). This method yielded 25 5 mL fractions: 15 fractions with 0% ethyl acetate in hexanes, 5 fractions with 5% ethyl acetate in hexanes, and 5 fractions with 20% ethyl acetate in hexane. (vii) We analyzed the fractions with thin-layer chromatography (TLC, 3:7 ethyl acetate/hexane) using vanillin acid—sulfuric acid as the detection method:  $\alpha$ -bisabolene appears as a dark blue spot on the TLC plates. Three fractions were enriched in  $\alpha$ -bisabolene. (viii) We combined these fractions and dried them with a rotary evaporator. (ix) We confirmed the final composition with <sup>1</sup>H NMR in CDCl<sub>3</sub> (Figure S16). The final spectrum is consistent with the published literature values. <sup>74</sup> The combined fractions contained >95% pure  $\alpha$ -bisabolene ( $^{1}$ H NMR).

**NMR Spectroscopy.** We carried out NMR spectroscopy at the BioFrontiers Nuclear Magnetic Resonance Facility at CU Boulder. We completed all experiments at 25 °C with a Bruker Accent 300 MHz spectrometer equipped with a Bruker 5 mm Smart Broadband Observe solution probe (BBFO), and we processed final spectra with MestReNova 14.2 software.

**Polarimetry.** The stereochemistry of (-)- $\alpha$ -bisabolol, (+)- $\alpha$ -bisabolol, (+)-epi- $\alpha$ -bisabolol, (-)- $\beta$ -bisabolol, and (-)- $\beta$ -bisabolene reflects stereochemistry or specific rotation values reported in vendor certificates. We determined the specific rotation of (+)- $\alpha$ -bisabolene by using an Anton Paar MCP-200 polarimeter. In brief, we used the sodium D line at 589 nm with a cell path length of 100 mm. For  $\alpha$ -bisabolene, we dissolved 12.18 mg of the colorless oil in 3.0 mL of CHCl<sub>3</sub>  $(0.406 \text{ g}/100 \text{ mL CHCl}_3)$ , placed the resulting solution inside the cell, and allowed the temperature to equilibrate to 25 °C before collecting a reading.

**Intracellular Metabolites.** We examined intracellular concentrations of terpenoids by extracting these compounds from cells grown in 4 mL cultures. Briefly, at 72 h, we removed 1 mL of cell culture, centrifuged it for 3 min (4000g), and discarded the supernatant. We extracted terpenoids from the cell pellet by adding 600  $\mu$ L of hexane and 100  $\mu$ L of 0.1 mm disrupter beads (Chemglass, CLS-1835-BG1) and vortexing the suspension for 30 min. We centrifuged the resulting lysate at 17,000g for 10 min and analyzed the resulting hexane layer using GC/MS as described above. Finally, we determined intracellular concentrations of each terpenoid ( $C_{\text{cell}}$ )

$$C_{\text{cell}} = \frac{C_{\text{culture}} \cdot V_{\text{hexane}}}{\eta \cdot \text{OD}_{600} \cdot C_{\text{OD}} \cdot V_{\text{cell}}}$$
(1)

by using eq 1, where  $C_{\rm culture}$  is the concentration of terpenoids in the hexane,  $V_{\rm hexane}$  is  $600~\mu{\rm L}$ ,  $\eta$  is the extraction efficiency,  $C_{\rm OD}$  is the OD-specific cell concentration (7.8 ×  $10^8$  cells mL $^{-1}$  OD $^{-1}$ ), and  $V_{\rm cell}$  is the volume of a single cell (4.4 fL/cell). For initial estimates, we used  $\eta=1$ , which assumes both complete cell lysis and complete partitioning of terpenoids from the aqueous to the organic layer; accordingly, our approach probably underestimates intracellular terpenoid concentrations.

**Protein Expression and Purification.** We overexpressed 3CLpro in *E. coli*. In brief, we transformed BL21(DE3) pLysS competent cells with a pGEX-4T-1 GST vector containing full-length 3CLpro with a 6x polyhistidine tag and a HRV 3C protease site on its C-terminus (i.e., Q\*GPHHHHHHH, where Q is the C-terminal residue of the protein and \* is the protease cleavage site). We used two colonies to inoculate two 10 mL liquid cultures (LB supplemented with 50  $\mu$ g/mL carbenicillin

and 34  $\mu$ g/mL chloramphenicol), which we grew overnight in an incubator shaker (37 °C and 200 rpm). We used these starter cultures to inoculate two one-liter cultures in 2.5 liter Ultra Yield Flasks, which we placed in an incubator shaker (37 °C and 200 rpm). At an OD<sub>600</sub> of 0.65, we lowered the temperature to 16 °C, induced protein expression by adding 0.5 mM dioxane-free IPTG, and grew the cultures for 18 h. We centrifuged final cultures, resuspended the pellets in 20 mL of lysis buffer (50 mM Tris, 1% Triton X-100, 300 mM NaCl, pH 8.0), and stored them at -80 °C.

We purified 3CLpro from cell pellets by using fast protein liquid chromatography (FPLC). To begin, we lysed the frozen cell pellets by adding the following solution to each: 120  $\mu$ L of Bond Breaker with 500 mM TCEP (Thermo Scientific), 100  $\mu$ g of lyophilized lysozyme (Thermo Scientific), 2 mL of BugBuster 10× protein extraction reagent (EMD Millipore), and 20  $\mu$ L of 25 U/ $\mu$ L benzonase (Millipore Sigma). We rocked these samples at room temperature for 1 h and spun them down at 16,000g for 25 min. We combined the supernatant from each lysis reaction, added imidazole (Teknova) to a final concentration of 5 mM, and filtered the final solution with 0.22  $\mu$ m Steriflip filter (Millipore Sigma). We loaded the filtered solution onto a 5 mL HisTrap HP column (Cytiva) using a GE Akta Purifier 10, washed the column with five column volumes of Tris buffer (50 mM Tris, 300 mM NaCl, 50 mM imidazole, 0.5 mM TCEP, pH 8.0), and eluted the protein with imidazole (50 to 200 mM imidazole). We used a 30 kDa Spin-X UF spin column (Corning) to concentrate the final protein to 10 mg/mL in cold HRV 3C protease cleavage buffer (50 mM Tris, 150 mM NaCl, 1 mM EDTA, 0.5 mM TCEP, pH 7.0). We added Rhinovirus 3C Protease (Thermo Pierce) at a ratio of 1 mg of HRV 3C protease for every 3 mg of 3CLpro and incubated the proteolysis reaction at 4 °C for 16 h. To remove the His-tagged HRV 3C protease and unproteolyzed 3CLpro, we diluted the final sample in Tris buffer (50 mM Tris, 300 mM NaCl, 0.5 mM TCEP, pH 8.0) to lower the imidazole concentration below 10 mM, loaded it onto a 5 mL HisTrap HP column, and collected the flowthrough. We filtered the final protein with a 0.45 µm filter, diluted it 20-fold into Tris buffer (25 mM pH 8.0), and loaded it onto an equilibrated 5 mL HiTrap Q-HP column (Cytiva). We washed the loaded column with five column volumes of Tris buffer (25 mM, pH 8.0) and eluted with salt (25 mM Tris, 500 mM NaCl, pH 8.0). We pooled fractions with 3CLpro, exchanged them into cold Tris buffer (50 mM Tris, 1 mM EDTA, 0.5 mM TCEP, pH 7.3), and concentrated the protein to >10 mg/mL with a 30 kDa cutoff Spin-X UF spin column prior to freezing at −80 °C.

**Enzyme Kinetics.** We characterized the inhibitory effects of various compounds by measuring their influence on 3CLprocatalyzed proteolysis of a fluorogenic peptide substrate (TSAVLQ\_AFC). Briefly, we prepared 100  $\mu$ L reactions consisting of 5  $\mu$ g/mL SARS-CoV-2 3CLpro, 10  $\mu$ g/mL TSAVLQ\_AFC, and 0.01–10,000  $\mu$ M terpenoid in HEPES buffer (25 mM, pH = 7.3) with 1% DMSO. We initiated these reactions by adding peptide substrate, and we monitored the proteolysis of fluorogenic peptide and subsequent liberation of the AFC fluorophore by measuring fluorescence ( $\lambda_{\rm ex}$  = 400 nm,  $\lambda_{\rm em}$  = 505 nm) every 10 s for 10 min (SpectraMax iD3 plate reader). Figure S18 provides our standard curve for AFC.

**Statistical Analysis and Reproducibility.** We determined statistical significance with a two-tailed Welch's *t*-test.

#### ASSOCIATED CONTENT

## **5** Supporting Information

The Supporting Information is available free of charge at https://pubs.acs.org/doi/10.1021/acssynbio.2c00384.

Studies of alternative B2H systems; results of drop-based plating experiments; analyses of the product profiles of terpenoid pathways; kinetic measurements; standard curves for terpenoid and fluorophore quantification; and tables describing gene sources, plasmids, B2H components, primers, growth conditions for *E. coli*, and terpenoid titers (PDF)

(Table S5) Titers of natural product pathways; measurements of titers, including error and sample sizes, for strains containing various biosynthetic pathways (XLSX) (Table S6) Kinetics of inhibition; the discrete kinetic measurements made in this study, including standard error and exact sample sizes (XLSX)

#### AUTHOR INFORMATION

#### **Corresponding Author**

Jerome M. Fox — Department of Chemical and Biological Engineering, University of Colorado, Boulder, Boulder, Colorado 80303, United States; orcid.org/0000-0002-3739-1899; Email: jerome.fox@colorado.edu

#### **Authors**

Levi Kramer – Department of Chemical and Biological Engineering, University of Colorado, Boulder, Boulder, Colorado 80303, United States

Ankur Sarkar — Department of Chemical and Biological Engineering, University of Colorado, Boulder, Boulder, Colorado 80303, United States

Tom Foderaro – Think Bioscience, Inc., Boulder, Colorado 80309, United States

Andrew L. Markley — Think Bioscience, Inc., Boulder, Colorado 80309, United States

Jessica Lee – Think Bioscience, Inc., Boulder, Colorado 80309, United States

Hannah Edstrom — Department of Chemical and Biological Engineering, University of Colorado, Boulder, Boulder, Colorado 80303, United States

Shajesh Sharma — Department of Chemical and Biological Engineering, University of Colorado, Boulder, Boulder, Colorado 80303, United States

Eden Gill — Department of Chemical and Biological Engineering, University of Colorado, Boulder, Boulder, Colorado 80303, United States

Matthew J. Traylor — Think Bioscience, Inc., Boulder, Colorado 80309, United States

Complete contact information is available at: https://pubs.acs.org/10.1021/acssynbio.2c00384

#### **Author Contributions**

L.K., A.S., and J.M.F. conceived of research and designed experiments. L.K. and A.S. assembled B2H systems, plasmids, and *E. coli* strains and carried out growth-coupled assays. M.J.T. designed the C-terminal extension of USP7. L.K. completed kinetic measurements, and L.K., M.J.T., and J.M.F. analyzed kinetic data. L.K. and S.S. completed luminescence assays. E.G. tested RBS sites for B2H systems. L.K., A.S., A.L.M., J.L., H.E., and M.J.T. carried out terpenoid production. A.S., A.L.M., and

T.F. extracted and analyzed terpenoids. T.F. purified  $\alpha$ -bisabolene. L.K. and J.M.F. wrote the paper.

#### Notes

The authors declare the following competing financial interest(s): L.K., A.S., T.F., A.L.M., H.E., M.J.T., and J.M.F. are inventors on patent applications that include data from this manuscript. J.M.F. is a founder of Think Bioscience, Inc., which employs L.K., A.S., T.F., A.L.M., J.L., M.J.T., and J.M.F., and which has licensed the intellectual property described in the aforementioned patent applications.

### ACKNOWLEDGMENTS

This work was supported by funds provided by the National Science Foundation (L.K., A.S., T.F., A.L.M., J.L., M.J.T., and J.M.F., 2030347; S.S. and E.G., 1750244), Think Bioscience (L.K., AWD-21-04-0032), and the National Institute of General Medical Sciences of the National Institutes of Health (H.E., R35GM143089).

#### REFERENCES

- (1) Bond, J. S. Proteases: History, Discovery, and Roles in Health and Disease. J. Biol. Chem. 2019, 294, 1643–1651.
- (2) Walsh, P. N.; Ahmad, S. S. Proteases in Blood Clotting. Essays Biochem. 2002, 38, 95–111.
- (3) Hiemstra, P. S. Novel Roles of Protease Inhibitors in Infection and Inflammation. *Biochem. Soc. Trans.* **2002**, *30*, 116–120.
- (4) Wellink, J.; van Kammen, A. Proteases Involved in the Processing of Viral Polyproteins. *Arch. Virol.* **1988**, *98*, 1–26.
- (5) Klemba, M.; Goldberg, D. E. Biological Roles of Proteases in Parasitic Protozoa. *Annu. Rev. Biochem.* **2002**, *71*, 275.
- (6) Ran, Y. L.; Zheng, S.; Tu, A. T. Biochemical Characterization of Two Hemorrhagic Proteases from the Venom of Lachesis Muta (Bushmaster). *Chem. Res. Toxicol.* **1988**, *1*, 337–342.
- (7) Babé, L. M.; Craik, C. S. Viral Proteases: Evolution of Diverse Structural Motifs to Optimize Function. *Cell* **1997**, *91*, 427–430.
- (8) Page, M. J.; Di Cera, E. Serine Peptidases: Classification, Structure and Function. *Cell. Mol. Life Sci.* **2008**, *65*, 1220–1236.
- (9) Neurath, H. Proteolytic enzymes past and present: The second golden era. *Protein Sci.* **1994**, *3*, 1734.
- (10) Urban, S.Rhomboid Intramembrane Serine Proteases. *Intra*membrane-Cleaving Proteases (I-CLiPs); Springer, 2007; pp 51–77.
- (11) Wang, Z.; Lv, Y.; Chu, Y. HIV Protease Inhibitors: A Review of Molecular Selectivity and Toxicity. *HIV AIDS* **2015**, *7*, 95.
- (12) Frick, D. N. The Hepatitis C Virus NS3 Protein: A Model RNA Helicase and Potential Drug Target. *Curr. Issues Mol. Biol.* **2007**, *9*, 1–20.
- (13) Wu, C.; Liu, Y.; Yang, Y.; Zhang, P.; Zhong, W.; Wang, Y.; Wang, Q.; Xu, Y.; Li, M.; Li, X.; Zheng, M.; Chen, L.; Li, H. Analysis of Therapeutic Targets for SARS-CoV-2 and Discovery of Potential Drugs by Computational Methods. *Acta Pharm. Sin. B* **2020**, *10*, 766–788.
- (14) Hua, Y.; Nair, S. Proteases in Cardiometabolic Diseases: Pathophysiology, Molecular Mechanisms and Clinical Applications. *Biochim. Biophys. Acta* **2015**, *18*52, 195.
- (15) Sippl, W.; Collura, V.; Colland, F. Ubiquitin-Specific Proteases as Cancer Drug Targets. *Future Oncol.* **2011**, *7*, 619–632.
- (16) Chen, Z.; Li, Y.; Schock, H. B.; Hall, D.; Chen, E.; Kuo, L. C. Three-Dimensional Structure of a Mutant HIV-1 Protease Displaying Cross-Resistance to All Protease Inhibitors in Clinical Trials. *J. Biol. Chem.* 1995, 270, 21433–21436.
- (17) Drag, M.; Salvesen, G. S. Emerging Principles in Protease-Based Drug Discovery. *Nat. Rev. Drug Discovery* **2010**, *9*, 690–701.
- (18) Wen, C. C.; Kuo, Y. H.; Jan, J. T.; Liang, P. H.; Wang, S. Y.; Liu, H. G.; Lee, C. K.; Chang, S. T.; Kuo, C. J.; Lee, S. S.; Hou, C. C.; Hsiao, P. W.; Chien, S. C.; Shyur, L. F.; Yang, N. S. Specific Plant Terpenoids and Lignoids Possess Potent Antiviral Activities against Severe Acute Respiratory Syndrome Coronavirus. *J. Med. Chem.* **2007**, *50*, 4087–4095.

- (19) Rubio-Martínez, J.; Jiménez-Alesanco, A.; Ceballos-Laita, L.; Ortega-Alarcón, D.; Vega, S.; Calvo, C.; Benítez, C.; Abian, O.; Velázquez-Campoy, A.; Thomson, T. M.; Granadino-Roldán, J. M.; Gómez-Gutiérrez, P.; Pérez, J. J. Discovery of Diverse Natural Products as Inhibitors of SARS-CoV-2 MproProtease through Virtual Screening. *J. Chem. Inf. Model.* **2021**, *61*, 6094—6106.
- (20) Macarron, R.; Banks, M. N.; Bojanic, D.; Burns, D. J.; Cirovic, D. A.; Garyantes, T.; Green, D. V. S.; Hertzberg, R. P.; Janzen, W. P.; Paslay, J. W.; Schopfer, U.; Sittampalam, G. S. Impact of High-Throughput Screening in Biomedical Research. *Nat. Rev. Drug Discovery* **2011**, *10*, 188–195.
- (21) Hubert, J.; Nuzillard, J. M.; Renault, J. H. Dereplication Strategies in Natural Product Research: How Many Tools and Methodologies behind the Same Concept? *Phytochem. Rev.* **2015**, *16*, 55–95.
- (22) Brooks, W. H.; Guida, W. C.; Daniel, K. J. The Significance of Chirality in Drug Design and Development. *Curr. Top. Med. Chem.* **2011**, *11*, 760.
- (23) Kautsar, S. A.; Blin, K.; Shaw, S.; Weber, T.; Medema, M. H. BiG-FAM: The Biosynthetic Gene Cluster Families Database. *Nucleic Acids Res.* **2021**, *49*, D490–D497.
- (24) Cimermancic, P.; Medema, M. H.; Claesen, J.; Kurita, K.; Wieland Brown, L. C.; Mavrommatis, K.; Pati, A.; Godfrey, P. A.; Koehrsen, M.; Clardy, J.; Birren, B. W.; Takano, E.; Sali, A.; Linington, R. G.; Fischbach, M. A. Insights into Secondary Metabolism from a Global Analysis of Prokaryotic Biosynthetic Gene Clusters. *Cell* **2014**, *158*, 412–421.
- (25) Rutledge, P. J.; Challis, G. L. Discovery of Microbial Natural Products by Activation of Silent Biosynthetic Gene Clusters. *Nat. Rev. Microbiol.* **2015**, *13*, 509–523.
- (26) Marchand, J. A.; Neugebauer, M. E.; Ing, M. C.; Lin, C. I.; Pelton, J. G.; Chang, M. C. Y. Discovery of a Pathway for Terminal-Alkyne Amino Acid Biosynthesis. *Nature* **2019**, *567*, 420–424.
- (27) Dachwitz, S.; Widmann, C.; Frese, M.; Niemann, H. H.; Sewald, N. Enzymatic Halogenation: Enzyme Mining, Mechanisms, and Implementation in Reaction Cascades. *Amino-Acids, Pept., Proteins* **2020**, *43*, 1–43.
- (28) Oinuma, K. I.; Takuwa, A.; Taniyama, K.; Doi, Y.; Takaya, N. Hydrazidase, a Novel Amidase Signature Enzyme That Hydrolyzes Acylhydrazides. *J. Bacteriol.* **2015**, *197*, 1115.
- (29) Chemat, F.; Abert-Vian, M.; Fabiano-Tixier, A. S.; Strube, J.; Uhlenbrock, L.; Gunjevic, V.; Cravotto, G. Green Extraction of Natural Products. Origins, Current Status, and Future Challenges. *TrAC, Trends Anal. Chem.* **2019**, *118*, 248–263.
- (30) Dubach, J. M.; Kim, E.; Yang, K.; Cuccarese, M.; Giedt, R. J.; Meimetis, L. G.; Vinegoni, C.; Weissleder, R. Quantitating Drug-Target Engagement in Single Cells in Vitro and in Vivo. *Nat. Chem. Biol.* **2016**, 13, 168–173.
- (31) Bunnage, M. E.; Chekler, E. L. P.; Jones, L. H. Target Validation Using Chemical Probes. *Nat. Chem. Biol.* **2013**, *9*, 195–199.
- (32) Butcher, E. C. Can cell systems biology rescue drug discovery? *Nat. Rev. Drug Discovery* **2005**, *4*, 461–467.
- (33) Oltvai, Z. N.; Barabási, A. L. Systems Biology: Life's Complexity Pyramid. *Science* **2002**, 298, 763–764.
- (34) Ideker, T.; Galitski, T.; Hood, L. A New Approach to Decoding Life: Systems Biology. *Annu. Rev. Genomics Hum. Genet.* **2001**, *2*, 343–372.
- (35) van der Greef, J.; McBurney, R. N. Rescuing Drug Discovery: In Vivo Systems Pathology and Systems Pharmacology. *Nat. Rev. Drug Discovery* **2005**, *4*, 961–967.
- (36) Dietrich, J. D.; McKee, J. A.; Keasling, A. E. High-Throughput Metabolic Engineering: Advances in Small-Molecule Screening and Selection. *Annu. Rev. Biochem.* **2010**, *79*, 563–590.
- (37) Martin, V. J. J.; Yoshikuni, Y.; Keasling, J. D. The in vivo synthesis of plant sesquiterpenes by Escherichia coli. *Biotechnol. Bioeng.* **2001**, *75*, 497–503.
- (38) Nielsen, J.; Keasling, J. D. Engineering Cellular Metabolism. *Cell* **2016**, *164*, 1185–1197.

- (39) Lee, S. Y.; Kim, H. U. Systems Strategies for Developing Industrial Microbial Strains. *Nat. Biotechnol.* **2015**, 33, 1061–1072.
- (40) McCall, J.; Kadam, S.; Katz, L. A High Capacity Microbial Screen for Inhibitors of Human Rhinovirus Protease 3C. *Bio/Technology* **1994**, *12*, 1012–1016.
- (41) Dautin, N.; Karimova, G.; Ullmann, A.; Ladant, D. Sensitive Genetic Screen for Protease Activity Based on a Cyclic AMP Signaling Cascade in Escherichia Coli. *J. Bacteriol.* **2000**, *182*, 7060–7066.
- (42) Balint, R. F.; Plooy, I. Protease-Dependent Streptomycin Sensitivity in E. coli-A System for Protease Inhibitor Selection. *Biotechnology* **1995**, *13*, 507–510.
- (43) Young, T. S.; Young, D. D.; Ahmad, I.; Louis, J. M.; Benkovic, S. J.; Schultz, P. G. Evolution of Cyclic Peptide Protease Inhibitors. *Proc Natl Acad Sci U.S.A.* **2011**, *108*, 11052–11056.
- (44) Debouck, C. The HIV-1 Protease as a Therapeutic Target for AIDS. AIDS Res Hum Retroviruses. 1992, 8, 153–164.
- (45) Wu, C.; Liu, Y.; Yang, Y.; Zhang, P.; Zhong, W.; Wang, Y.; Wang, Q.; Xu, Y.; Li, M.; Li, X.; Zheng, M.; Chen, L.; Li, H. Analysis of Therapeutic Targets for SARS-CoV-2 and Discovery of Potential Drugs by Computational Methods. *Acta Pharm. Sin. B* **2020**, *10*, 766–788.
- (46) McClain, C. B.; Vabret, N. SARS-CoV-2: The Many Pros of Targeting PLpro. Signal Transduction Targeted Ther. 2020, 5, 223.
- (47) Wang, Z.; Kang, W.; You, Y.; Pang, J.; Ren, H.; Suo, Z.; Liu, H.; Zheng, Y. USP7: Novel Drug Target in Cancer Therapy. Front. Pharmacol. 2019, 10, 427.
- (48) Volontè, F.; Piubelli, L.; Pollegioni, L. Optimizing HIV-1 Protease Production in Escherichia Coli as Fusion Protein. *Microb. Cell Fact.* **2011**, *10*, 53.
- (49) Xue, X.; Yang, H.; Shen, W.; Zhao, Q.; Li, J.; Yang, K.; Chen, C.; Jin, Y.; Bartlam, M.; Rao, Z. Production of Authentic SARS-CoV Mpro with Enhanced Activity: Application as a Novel Tag-cleavage Endopeptidase for Protein Overproduction. *J. Mol. Biol.* **2007**, 366, 965–975.
- (50) Shin, D.; Mukherjee, R.; Grewe, D.; Bojkova, D.; Baek, K.; Bhattacharya, A.; Schulz, L.; Widera, M.; Mehdipour, A. R.; Tascher, G.; Geurink, P. P.; Wilhelm, A.; van der Heden van Noort, G. J.; Ovaa, H.; Müller, S.; Knobeloch, K. P.; Rajalingam, K.; Schulman, B. A.; Cinatl, J.; Hummer, G.; Ciesek, S.; Dikic, I. Papain-like Protease Regulates SARS-CoV-2 Viral Spread and Innate Immunity. *Nature* 2020, 587, 657–662.
- (51) Rougé, L.; Bainbridge, T. W.; Kwok, M.; Tong, T.; Di Lello, P.; Wertz, I. E.; Maurer, T.; Ernst, J. A.; Murray, J. Molecular Understanding of USP7 Substrate Recognition and C-Terminal Activation. *Structure* **2016**, *24*, 1335–1345.
- (52) Carpenter, A. C.; Paulsen, I. T.; Williams, T. C. Blueprints for Biosensors: Design, Limitations, and Applications. *Genes* **2018**, *9*, 375.
- (53) Sarkar, A.; Kim, E. Y.; Jang, T.; Hongdusit, A.; Kim, H.; Choi, J. M.; Fox, J. M. Microbially Guided Discovery and Biosynthesis of Biologically Active Natural Products. *ACS Synth. Biol.* **2021**, *10*, 1505–1510
- (54) Carlson, J. C.; Badran, A. H.; Guggiana-Nilo, D. A.; Liu, D. R. Negative Selection and Stringency Modulation in Phage-Assisted Continuous Evolution. *Nat. Chem. Biol.* **2014**, *10*, 216–222.
- (55) Barretto, N.; Jukneliene, D.; Ratia, K.; Chen, Z.; Mesecar, A. D.; Baker, S. C. The Papain-Like Protease of Severe Acute Respiratory Syndrome Coronavirus Has Deubiquitinating Activity. *J. Virol.* **2005**, 79, 15189–15198.
- (56) Nicholson, B.; Suresh Kumar, K. G. The Multifaceted Roles of USP7: New Therapeutic Opportunities. *Cell Biochem. Biophys.* **2011**, *60*, *61*–*68*.
- (57) Rut, W.; Lv, Z.; Zmudzinski, M.; Patchett, S.; Nayak, D.; Snipas, S. J.; El Oualid, F.; Huang, T. T.; Bekes, M.; Drag, M.; Olsen, S. K. Activity Profiling and Crystal Structures of Inhibitor-Bound SARS-CoV-2 Papain-like Protease: A Framework for Anti—COVID-19 Drug Design. *Sci. Adv.* **2020**, *6*, No. eabd4596.
- (S8) Beck, Z. Q.; Morris, G. M.; Elder, J. H. Defining HIV-1 Protease Substrate Selectivity. *Curr. Drug Targets: Infect. Disord.* **2002**, *2*, 37–50.
- (59) Leung, D.; Abbenante, G.; Fairlie, D. P. Protease Inhibitors: Current Status and Future Prospects. J. Med. Chem. 2000, 43, 305–341.

**ACS Synthetic Biology** Research Article pubs.acs.org/synthbio

- (60) Johnson, S. R.; Bhat, W. W.; Sadre, R.; Miller, G. P.; Garcia, A. S.; Hamberger, B. Promiscuous Terpene Synthases from Prunella Vulgaris Highlight the Importance of Substrate and Compartment Switching in Terpene Synthase Evolution. New Phytol. 2019, 223, 323-335.
- (61) Major, D. T.; Weitman, M. Electrostatically Guided Dynamicsthe Root of Fidelity in a Promiscuous Terpene Synthase? J. Am. Chem. Soc. 2012, 134, 19454-19462.
- (62) Owen, D. R.; Allerton, C. M. N.; Anderson, A. S.; Aschenbrenner, L.; Avery, M.; Berritt, S.; Boras, B.; Cardin, R. D.; Carlo, A.; Coffman, K. J.; Dantonio, A.; Di, L.; Eng, H.; Ferre, R. A.; Gajiwala, K. S.; Gibson, S. A.; Greasley, S. E.; Hurst, B. L.; Kadar, E. P.; Kalgutkar, A. S.; Lee, J. C.; Lee, J.; Liu, W.; Mason, S. W.; Noell, S.; Novak, J. J.; Obach, R. S.; Ogilvie, K.; Patel, N. C.; Pettersson, M.; Rai, D. K.; Reese, M. R.; Sammons, M. F.; Sathish, J. G.; Singh, R. S. P.; Steppan, C. M.; Stewart, A. E.; Tuttle, J. B.; Updyke, L.; Verhoest, P. R.; Wei, L.; Yang, Q.; Zhu, Y. An oral SARS-CoV-2 M pro inhibitor clinical candidate for the treatment of COVID-19. Science 2021, 374, 1586-1593.
- (63) Liu, H.; Iketani, S.; Zask, A.; Khanizeman, N.; Bednarova, E.; Forouhar, F.; Fowler, B.; Hong, S. J.; Mohri, H.; Nair, M. S.; Huang, Y.; Tay, N. E. S.; Lee, S.; Karan, C.; Resnick, S. J.; Quinn, C.; Li, W.; Shion, H.; Xia, X.; Daniels, J. D.; Bartolo-Cruz, M.; Farina, M.; Rajbhandari, P.; Jurtschenko, C.; Lauber, M. A.; McDonald, T.; Stokes, M. E.; Hurst, B. L.; Rovis, T.; Chavez, A.; Ho, D. D.; Stockwell, B. R. Development of Optimized Drug-like Small Molecule Inhibitors of the SARS-CoV-2 3CL Protease for Treatment of COVID-19. Nat. Commun. 2022, 13,
- (64) Huang, Q.; Williams, H. J.; Roessner, C. A.; Scott, A. I. Sesquiterpenes Produced by Truncated Taxadiene Synthase. Tetrahedron Lett. 2000, 41, 9701-9704.
- (65) Naumann, T. A.; Tavassoli, A.; Benkovic, S. J. Genetic Selection of Cyclic Peptide Dam Methyltransferase Inhibitors. ChemBioChem 2008, 9, 194-197.
- (66) Gadotti, V. M.; Huang, S.; Zamponi, G. W. The Terpenes Camphene and Alpha-Bisabolol Inhibit Inflammatory and Neuropathic Pain via Cav3.2 T-Type Calcium Channels. Mol. Brain 2021, 14, 166.
- (67) Sarkar, A.; Kim, E. Y.; Jang, T.; Hongdusit, A.; Kim, H.; Choi, J. M.; Fox, J. M. Microbially Guided Discovery and Biosynthesis of Biologically Active Natural Products. ACS Synth. Biol. 2021, 10, 1505-1519.
- (68) Sarria, S.; Wong, B.; García Martín, H.; Keasling, J. D.; Peralta-Yahya, P. Microbial Synthesis of Pinene. ACS Synth. Biol. 2014, 3, 466— 475.
- (69) Koo, H. J.; Gang, D. R. Suites of Terpene Synthases Explain Differential Terpenoid Production in Ginger and Turmeric Tissues. PLoS One 2012, 7, No. e51481.
- (70) Diaz, J. E.; Lin, C. S.; Kunishiro, K.; Feld, B. K.; Avrantinis, S. K.; Bronson, J.; Greaves, J.; Saven, J. G.; Weiss, G. A. Computational Design and Selections for an Engineered, Thermostable Terpene Synthase. Protein Sci. 2011, 20, 1597–1606.
- (71) Tinikul, R.; Chaiyen, P. Structure, Mechanism, and Mutation of Bacterial Luciferase. Adv. Biochem. Eng./Biotechnol. 2014, 154, 47-74.
- (72) Sawant, N.; Singh, H.; Appukuttan, D. Overview of the Cellular Stress Responses Involved in Fatty Acid Overproduction in E. Coli. Mol. Biotechnol. 2021, 64, 373-387.
- (73) Sarkar, A.; Foderaro, T.; Kramer, L.; Markley, A. L.; Lee, J.; Traylor, M. J.; Fox, J. M. Evolution-Guided Biosynthesis of Terpenoid Inhibitors. ACS Synth. Biol. 2022, 11, 3015-3027.
- (74) Peralta-Yahya, P. P.; Ouellet, M.; Chan, R.; Mukhopadhyay, A.; Keasling, J. D.; Lee, T. S. Identification and Microbial Production of a Terpene-Based Advanced Biofuel. Nat. Commun. 2011, 2, 483.
- (75) Volkmer, B.; Heinemann, M. Condition-Dependent Cell Volume and Concentration of Escherichia Coli to Facilitate Data Conversion for Systems Biology Modeling. PLoS One 2011, 6, No. e23126.
- (76) Tamura, K.; Stecher, G.; Kumar, S. MEGA11: Molecular Evolutionary Genetics Analysis Version 11. Molecular Biology and Evolution 2021, 38 (7), 3022-3027.

## **□** Recommended by ACS

**Autoinduction AND Gate Inhibits Cell Lysis to Enhance** Protein Production in Bacillus subtilis Controlled by Population Density and Cell Physiological State

Kuidong Xu, Song Liu, et al. MARCH 07, 2023

ACS SYNTHETIC BIOLOGY

Mechanistic Insights into Cell-Free Gene Expression through an Integrated -Omics Analysis of Extract Processing Methods

Blake J. Rasor, Michael C. Jewett, et al.

JANUARY 26, 2023

ACS SYNTHETIC BIOLOGY

READ **C** 

**Coupling Cell Communication and Optogenetics:** Implementation of a Light-Inducible Intercellular System in **Veast** 

Vicente Rojas and Luis F. Larrondo

DECEMBER 19 2022

ACS SYNTHETIC BIOLOGY

READ **C** 

## Signal Peptide Efficiency: From High-Throughput Data to **Prediction and Explanation**

Stefano Grasso, Tjeerd van Rij, et al.

JANUARY 17, 2023

ACS SYNTHETIC BIOLOGY

RFAD 🗹

Get More Suggestions >